Supplementary Information

The role of surface charge in the interaction of nanoparticles with model pulmonary surfactants

F. Mousseau[*] and J.-F. Berret[*]

Corresponding authors: fanny.mousseau@univ-paris-diderot.fr;
jean-francois.berret@univ-paris-diderot.fr

Supplementary Information   Table S1 – Curosurf® composition in lipids and proteins

Lipid composition (%, g/g of total lipid)	Native Surfactant	Curosurf
Phosphatidylcholine (PC)	70 - 85	67 - 74
Lysophosphatidyl choline (LPC)	0.5	< 1
Sphingomyelin(SM)	2	8.1
Cholesterol	5	0
Phosphatidylinositol (PI)	4 – 7	3.3
Phosphatidylserine (PS)	5	
Phosphatidylethanolamine (PE)	3	4.5
Phosphatidylglycerol (PG)	7 – 10	1.2
Protein concentration (%, g/g of total lipid)	**Native Surfactant**	**Curosurf**
SP-A	4	0
SP-B	1	0.3
SP-C	1	0.7
SP-D	4	0

Table S1: Lipid and protein compositions of native surfactant obtained by saline bronchoalveolar lavage compared to that of Curosurf®, a pulmonary surfactant substitute indicated for the rescue treatment of Respiratory Distress Syndrome (RDS) in premature infants [1-3].

Supplementary Information S1 – Curosurf® labeling

Curosurf® vesicles are stained by the fluorescent molecule PKH67 by simple mixing. Curosurf (resp. PKH 67) was diluted with DI-water at 2 g L^{-1} (resp. 2×10^{-6} M) and mixed rapidly at equal volumes. Optical microscopy images in Figure S2a and S2b shows that PKH67 addition in a ratio 1:1400 with respect to Curosurf® leads to vesicle staining. In Figures S2c and S2d, it is shown that labeling does not affect the vesicle size and zeta potential. Finally, interaction strength measurements using the scattering Job plot approach were found to yield similar S_{Int}-values for vesicles with and without dye molecules at 25 °C and 37 °C (Figure S2e). From these above results, it was concluded that the fluorescent Curosurf® has membrane properties similar to that of the native surfactant.
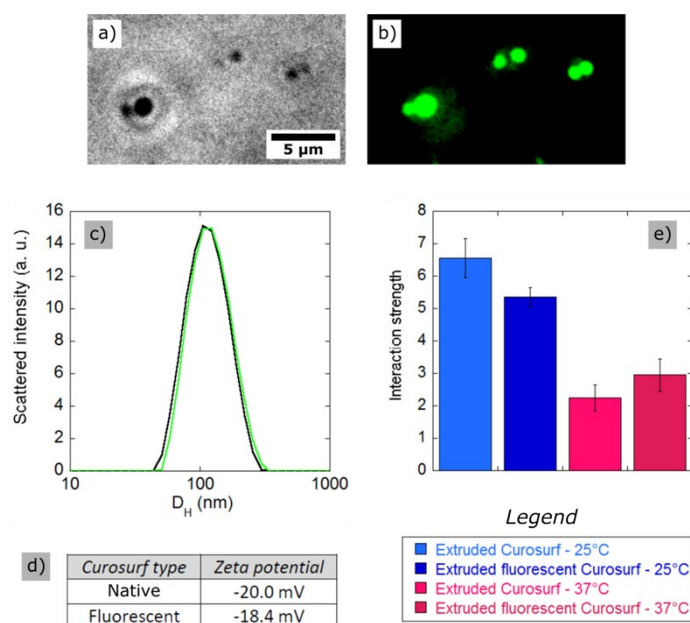

Figure S1 : a,b) Images of fluorescently labeled Curosurf® observed by optical microscopy in phase contrast (a) and fluorescence (b). c) Size distribution of native Curosurf® (continuous line) and fluorescent Curosurf® (continuous green line) obtained by DLS measurement. d) Zeta potential of native and fluorescent Curosurf®. e) Interaction strength obtained from the Job plot of Silica (+) / extruded Curosurf® at 25 °C and 37 °C for PKH67-labeled and non-labeled extruded Curosurf®.

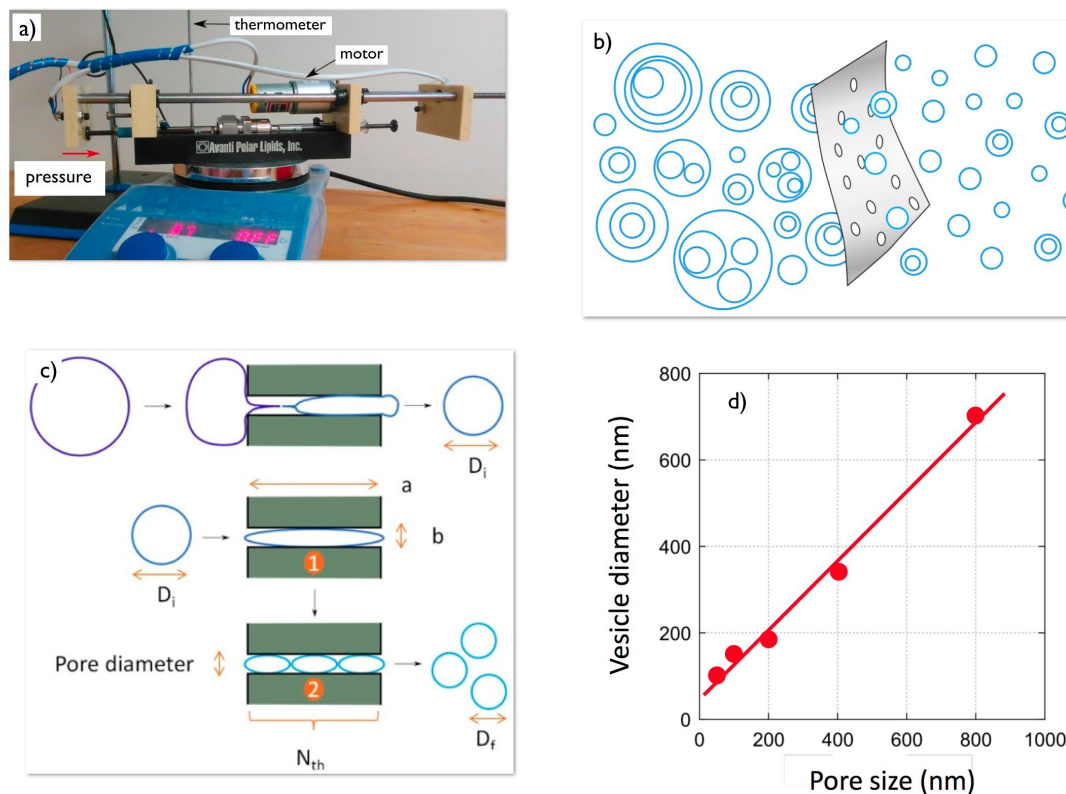# Supplementary Information S2 – Modeling the extrusion process and vesicle diameter as a function of the pore size

Figure S2: *a) Device used for extruding phospholipid dispersions using polycarbonate filter with controlled pore size. b) Schematic illustration of the extrusion process. c) Modeling the extrusion process: A two-steps model was developed to describe the extrusion of Curosurf® [4]. This model assumes that in the first passages, micron size vesicles are blocked at the pore entries, causing strong deformation and membrane breakings. For later passages, the vesicles are sheared and stretched in the pores, leading to a Rayleigh-like instability, and causing MLVs fragmentation into objects of diameter of the order of the pore size. d) Vesicle size dependence as a function of the pore size. The sizes were obtained from dynamic light scattering [5].*

Supplementary Information S3 – Additional cryo-TEM images of Curosurf® vesicles
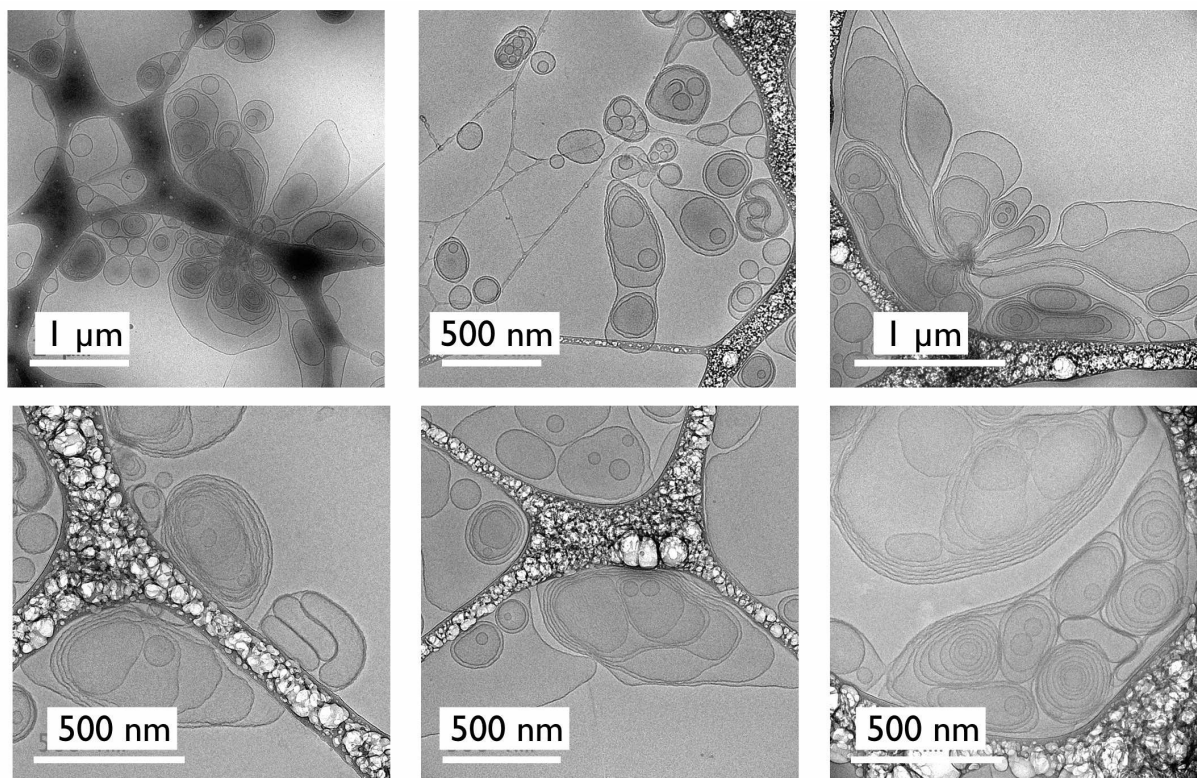

Figure S3: *Cryo-TEM images of Curosurf® vesicles at the concentration of 5 g L^{-1}.*

Supplementary Information S4 – Determination of Curosurf® vesicle membrane thickness and size from cryo-TEM
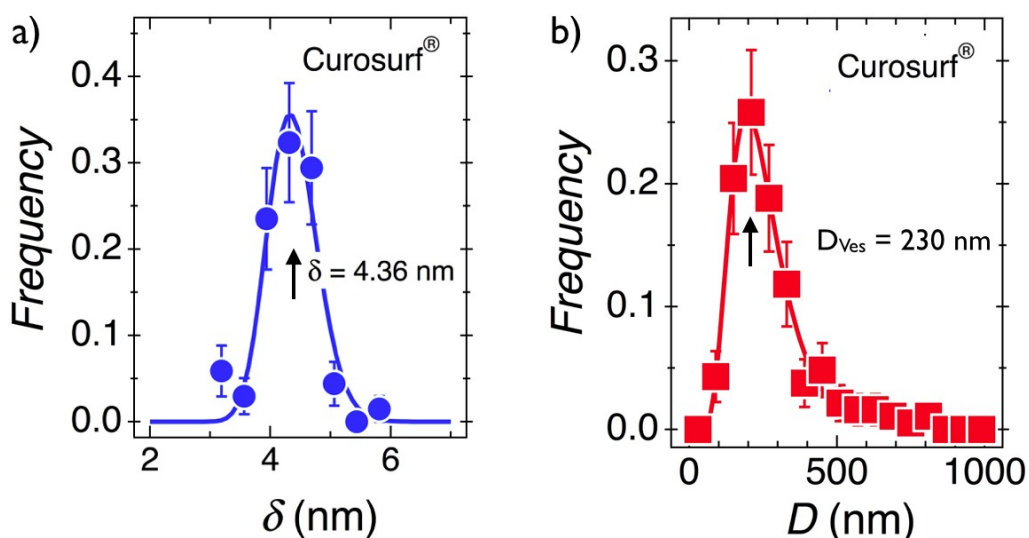

Figure S4: a) Distribution of Curosurf® membrane thickness obtained by cryo-TEM. The average value is δ = 4.36 nm. The distribution was determined on n = 68 measurements. b) Size distributions of Curosurf® vesicles obtained by cryo-TEM. For the vesicles, the size of each of the enclosed structures has been included into the statistical analysis. For large objects, corrections associated to the vesicle distortions were not taken into account. The distribution is well accounted for by a log-normal function of median 230 nm and dispersity 0.55.

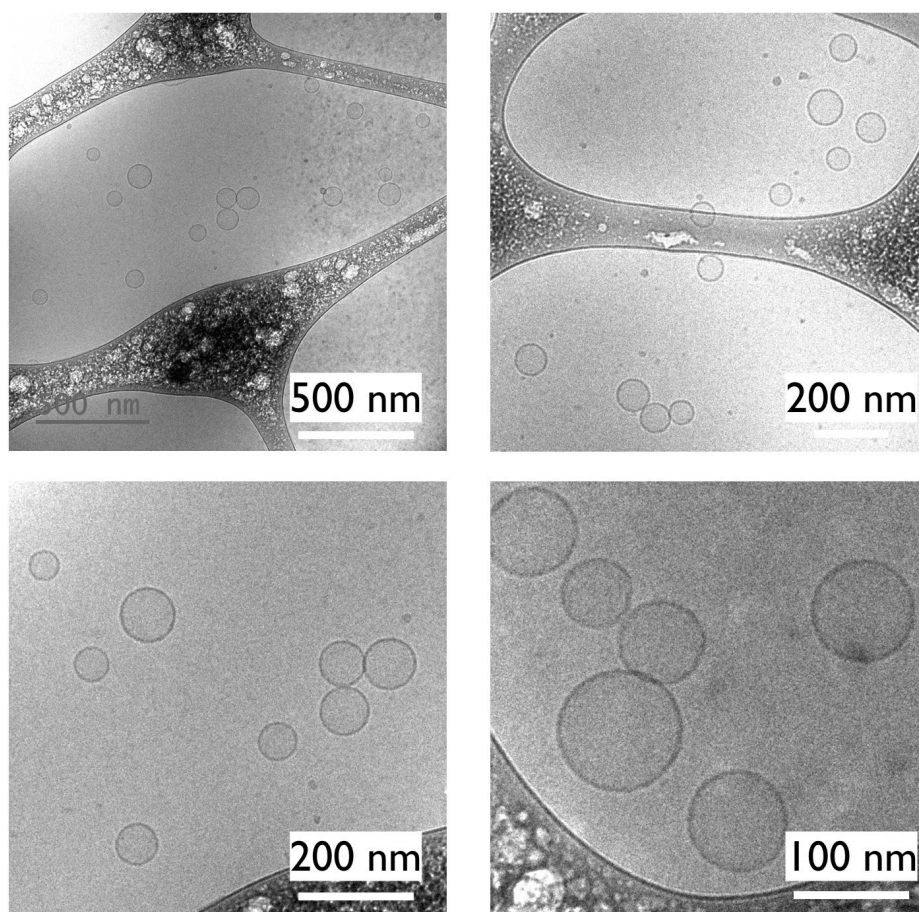# Supplementary Information S5 – Additional cryo-TEM images of extruded Curosurf® vesicles

500 nm · 200 nm · 200 nm · 100 nm

Figure S5: Cryo-TEM images of extruded Curosurf® vesicles at concentration 1 g L^{-1} obtained with a polycarbonate membrane with pore sizes 100 nm.

Supplementary Information Table S2 – Derivation of the Job scattering assuming SLB formation between nanoparticles and pulmonary surfactant vesicles

1 - Nanoparticles

Below are listed the parameters describing the structure and surface properties of the nanoparticles.

Nanoparticle parameters	Variable	Units
Median cryo-TEM diameter	D_{NP}	nm
Dispersity	s_{NP}	
Mass density	ρ	g cm^{-3}
Number-average molecular weight	M^{NP}_n	g mol^{-1}
Weight-average molecular weight	M^{NP}_w	g mol^{-1}
Molecular-weight dispersity	$Đ_{NP}$	
Nanoparticle concentration	c_{NP}	g L^{-1}
Number density of particles	n_{NP}	L^{-1}
Surface area concentration	c^s_{NP}	cm^2 L^{-1}

Table S2a: *List of the nanoparticle parameters used.*

For a dispersion of concentration c_{NP} (g L^{-1}), the number density of particles n_{NP} is given by:

$$n_{NP} = \frac{c_{NP}}{M^{NP}_n} N_A$$

where M^{NP}_n is the particle number-average molecular weight and N_A the Avogadro number.

The number-average molecular weight M^{NP}_n reads:

$$M^{NP}_n = \frac{\pi}{6} \rho D^3_{NP} exp\left(4.5 s^2_{NP}\right) N_A$$

For log-normal distribution of median diameter D_{NP} and dispersity s, the nth-moment is given by the expression $<D^n_{NP}> = \left(D^0_{NP}\right)^n exp(n^2 s^2/2)$. D^0_{NP} denotes here the median diameter. With the two above equations, we infer the number density of particles noted n_{NP} at a given concentration:

$$n_{NP} = \frac{6c_{NP}}{\pi \rho D_{NP}^3} exp\left(-4.5s_{NP}^2\right)$$

Assuming that the average surface developed by the particle is $\pi\left(D_{NP}^0\right)^2 exp\left(2s_{NP}^2\right)$, the Surface area concentration expresses as:

$$c_{NP}^s = A_{NP}c_{NP} = \frac{6c_{NP}}{\rho D_{NP}} exp\left(-2.5s_{NP}^2\right)$$

where A_{NP} is the specific surface area (in cm² g⁻¹). According to the previous equation, 1 mL of a nanoparticle dispersion at 1 g L⁻¹ (D_{NP} = 50 nm, ρ = 2 g cm⁻³) corresponds to a nominal surface of 600 cm² [5].

2 – Phospholipid vesicles

For molecular calculations, pulmonary surfactant bilayers are assumed to be similar to those made of dipalmitoylphosphatidylcholine (DPPC). In the following we assume that the number molecular weight of the lipid is 734 g mol⁻¹, and that the surface per head group is 0.60 nm² [2]. For the light scattering calculation, we consider vesicles uniform in size of diameter D_{Ves}.

Phospholipid concentration	c_{PL}	g L⁻¹
Phospholipid molecular weight	M_n^{PL}	g mol⁻¹
Phospholipid polar head surface	s_{PL}	nm²
Number density of lipids	n_{PL}	L⁻¹
Vesicle concentration	c_{Ves}	g L⁻¹
Vesicle diameter	D_{Ves}	nm
Number-average molecular weight	M_n^{Ves}	g mol⁻¹
Weight-average molecular weight	M_w^{Ves}	g mol⁻¹
Number density of vesicles	n_{Ves}	L⁻¹
Surface area concentration	c_{Ves}^s	cm² L⁻¹

Table S2b: *Phospholipid and vesicle characteristics.*

For a DPPC dispersion at concentration c_{PL}, the number density n_{PL} of phospholipids is given by:

$$n_{PL} = \frac{c_{PL}}{M_n^{PL}} N_A$$

Assuming a surface per polar head of s_{PL}, one gets for vesicle surface area concentration:

$$c_{Ves}^s = n_{PL}s_{PL}/2 \; = \; A_{Ves}c_{Ves} \qquad (S7.1)$$

In Eq. S7.1, the factor 2 arises from the fact that vesicles are made from bilayers and a bilayer cannot coat two different particles. A_{Ves} is the specific surface area. 1 mL of a DPPC dispersion at 1 g L^{-1} corresponds to $c_{Ves}^s = 2460$ cm^2 [2].

3 – Nanoparticle – Vesicle dispersions

Concentrations

In the Job scattering diagram considered, the nanoparticles are on the left-hand side and the vesicles on the right-hand side. The mixing is done using stock solutions at the same concentration c_0. The concentration of the different species in the Job scattering diagram will be:

$$c_{NP}(X) = \frac{1}{1+X}c_0$$

$$c_{Ves}(X) = \frac{X}{1+X}c_0$$

where $X = c_{Ves}/c_{NP}$ is the mixing ratio.

Surface ratio

For particles and phospholipids mixed at the same concentration, the surface ratio X_S can be expressed as a function of X:

$$X_S = \frac{c_{Ves}^s}{c_{NP}^s} = \frac{A_{Ves}}{A_{NP}}X$$

At X_S = 1, the surface area concentrations are equal. This corresponds to the critical X value, noted X_C:

$$X_C = \frac{A_{NP}}{A_{Ves}}$$

In case of supported lipid bilayer formation, all particles are covered with a membrane at $X = X_C$.

Scattering for non interacting species

At $X = 0$, the scattering intensity for the particles reads [6-8]:

$$I_{NP} = K_{NP} \, M_w^{NP} c_{NP}$$

Similarly, for the vesicles:

$$I_{Ves} = K_{Ves} \, M_w^{Ves} c_{Ves}$$

In the above expressions K_{NP} and K_{Ves} are the scattering contrasts for the nanoparticles and vesicles respecively. The form factors are neglected for sake of simplicity. For the mixed solutions, the scattering intensity is the sum of the particle and vesicle respective contributions, leading to:

$$I_{non-Inter}(c_0,X) = K_{NP} \, M_w^{NP} \frac{c_0}{1+X} + K_{Ves} \, M_w^{Ves} \frac{Xc_0}{1+X} \qquad (S7.2\,)$$

Scattering model SLB formation

Below X_c

In case of SLB formation, it is here assumed that all the vesicles present reorganize and associate with the particles. The scattering function arises from the sum of the coated and uncoated. The scattering intensity then reads:

$$I_{SLB}(c_0,X < X_c) = K_{NP} \, M_w^{NP} \frac{c_0}{1+X}\left(1 - \frac{X}{X_c}\right) + K_{SLB} \, M_w^{SLB} \frac{c_0 X}{X_c(1+X)}$$

where $M_w^{SLB} = M_w^{NP}(1+X_c)$, and K_{SLB} the scattering contrast for the SLB-coated particles.

Above X_c

Here all the particles present are coated with a SLB and coexist with the remaining vesicles. Above X_c, the scattering function reads:

$$I_{SLB}(c_0,X > X_c) = K_{SLB} \, M_w^{SLB} \frac{c_0}{1+X} + K_{Ves} \, M_w^{Ves} \frac{c_0}{(1+X)}(X - X_c)$$

Combining predictions below and above X_c

As a result, it is possible to predict the intensity arising from SLB-coated particles in the configuration of the Job scattering diagram.

$$I_{SLB}(c_0,X) = K_{NP} \, M_w^{NP} \frac{c_0}{1+X}\left(1 - \frac{X}{X_c}\right) + K_{SLB} \, M_w^{SLB} \frac{c_0 X}{X_c(1+X)} +$$

$$K_{SLB} \, M_w^{SLB} \frac{c_0}{1+X} + K_{Ves} \, M_w^{Ves} \frac{c_0}{(1+X)}(X - X_c) \qquad (S7.3)$$

Results

Eq. S7.3 has been estimated for different sets of parameters:

Nanoparticles	D_{NP} = 40 nm, s_{NP} = 0, ρ = 2 g cm^{-3}
Vesicles	D_{Ves} = 100 and 200 nm
Scattering contrast	K_{NP} = 1 - K_{Ves} = 1 - K_{SLB} = 1
	K_{NP} = 1 - K_{Ves} = 2 - K_{SLB} = 1.2
	K_{NP} = 1 - K_{Ves} = 0.5 - K_{SLB} = 0.8
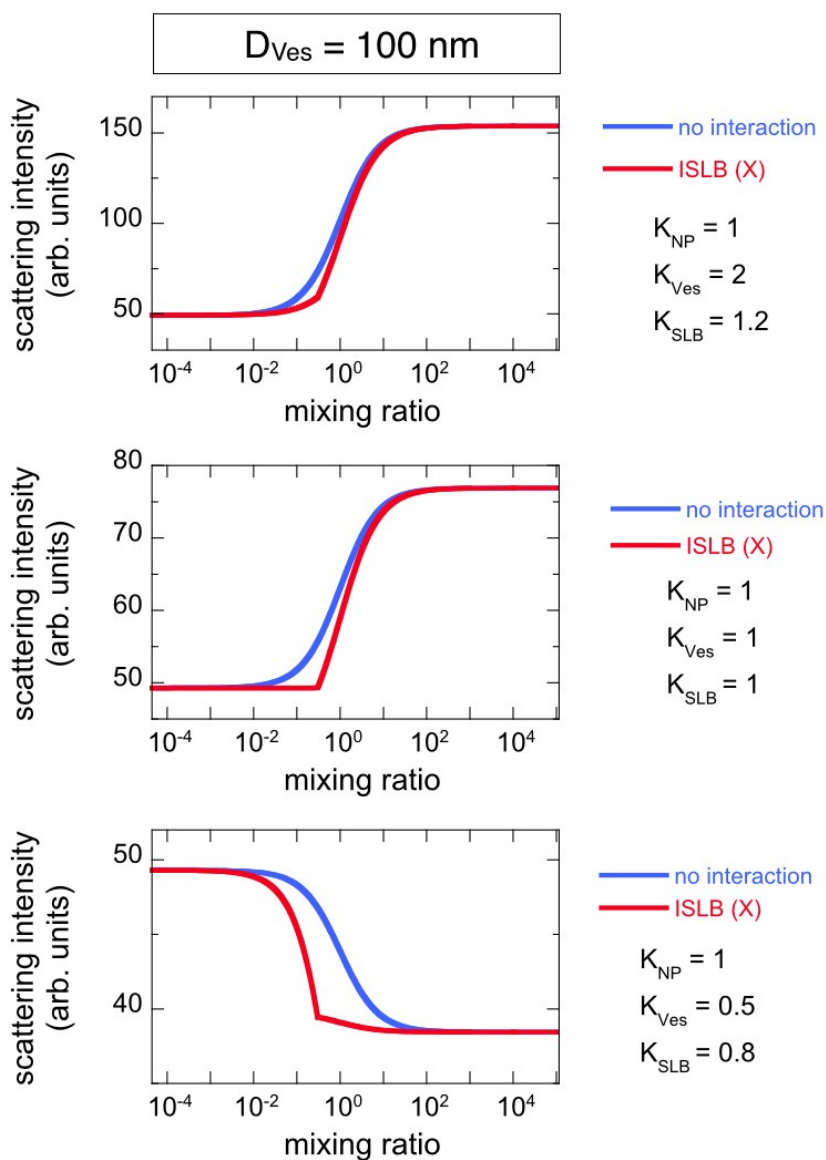
Figure S6.1: *Scattering intensity of 40 nm nanoparticle and 100 nm vesicle dispersions as a function of the mixing ratio X for the model on non-interacting species (blue) and for the model of SLB formation (red). The experimental conditions are such as $X = c_{Ves}/c_{NP}$. Note that for the different conditions, the scattering intensity for the SLB formation remains below that of the non-interacting species.*
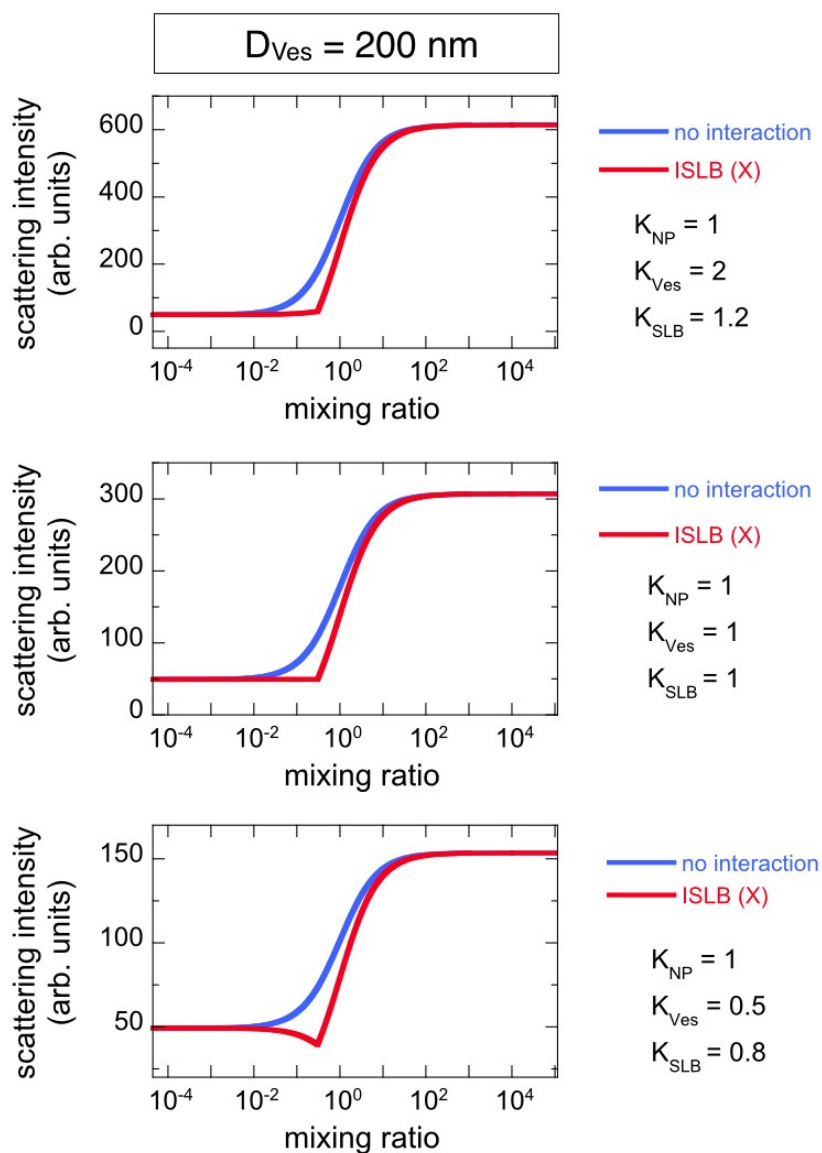
Figure S6.2: Same as in Fig. S7.1 for 40 nm nanoparticle and 200 nm vesicle dispersions.

Supplementary Information Figure S7 – Liquid-Gel transition from the Curosurf® phospholipid bilayer
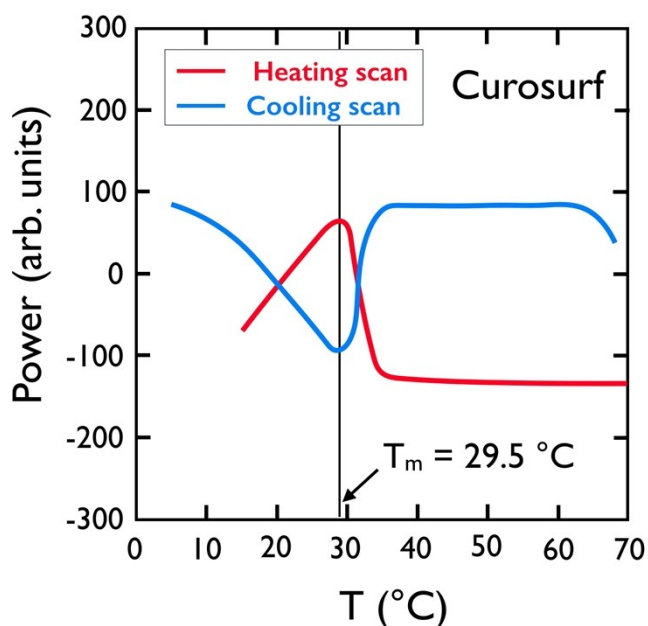
Figure S7: *Thermograms of Curosurf® diluted in DI-water at 10 g L^{-1} obtained by differential scanning calorimetry (DSC). The Curosurf® bilayer melting temperature was estimated at T_m = 29.5 °C from heating and cooling cycles. Thermograms were measured using an N-DSCIII instrument from CSC. The reference cell was filled with Milli-Q water and the sample cell (0.3 mL) with Curosurf®. The capillary cells were not capped and a constant pressure of 5×10^5 Pa was applied. The transition temperature was taken at the second, third and fourth heating scans, at a scan rate of 0.5 °C min^{-1} (from 5 to 70 °C). The melting temperature was estimated as the mean of the three transition temperatures mentioned before. The same procedure was applied with the cooling scans, which were performed in the same conditions.*

Supplementary Information Figure S8 – Job scattering plots of nanoparticle-vesicle dispersions at 25 °C
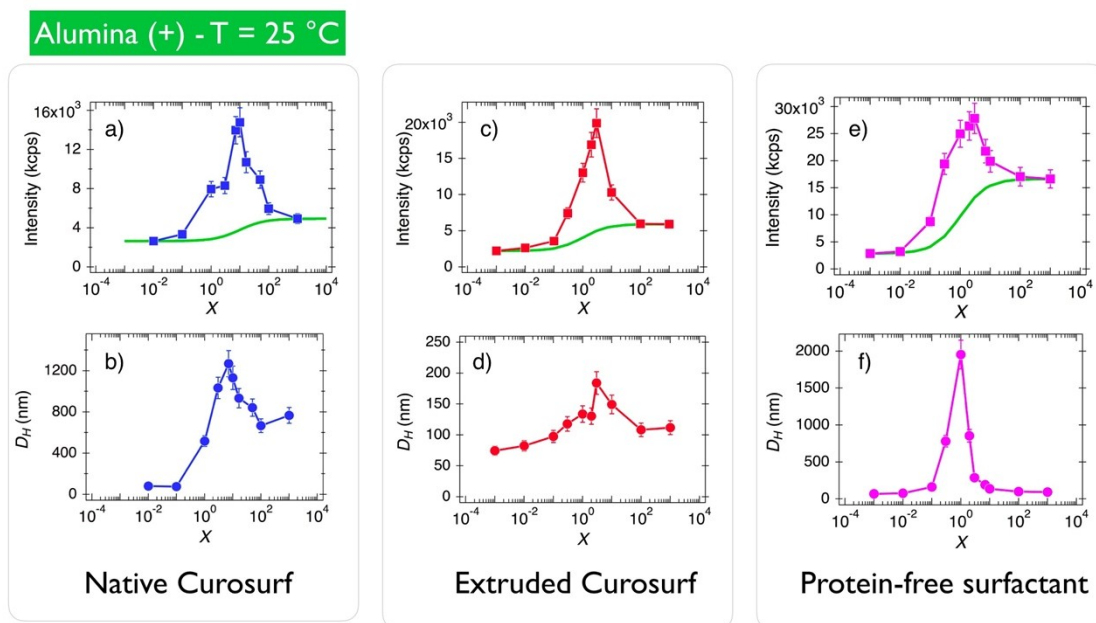
Figure S8.1: *Scattered intensity (a, c and e) and hydrodynamic diameter (b, d and f) of alumina particles mixed with native Curosurf® (a, b), extruded Curosurf® (c, d) and protein-free surfactant and (e, f) as a function of X (T = 25 °C). X is the ratio between the surfactant and nanoparticles weight concentration. The error bars represent the mean of the standard deviations for measurements made in triplicate. Continuous lines in green in a, c and e represent the scattered intensities calculated assuming that particles and vesicles do not interact.*
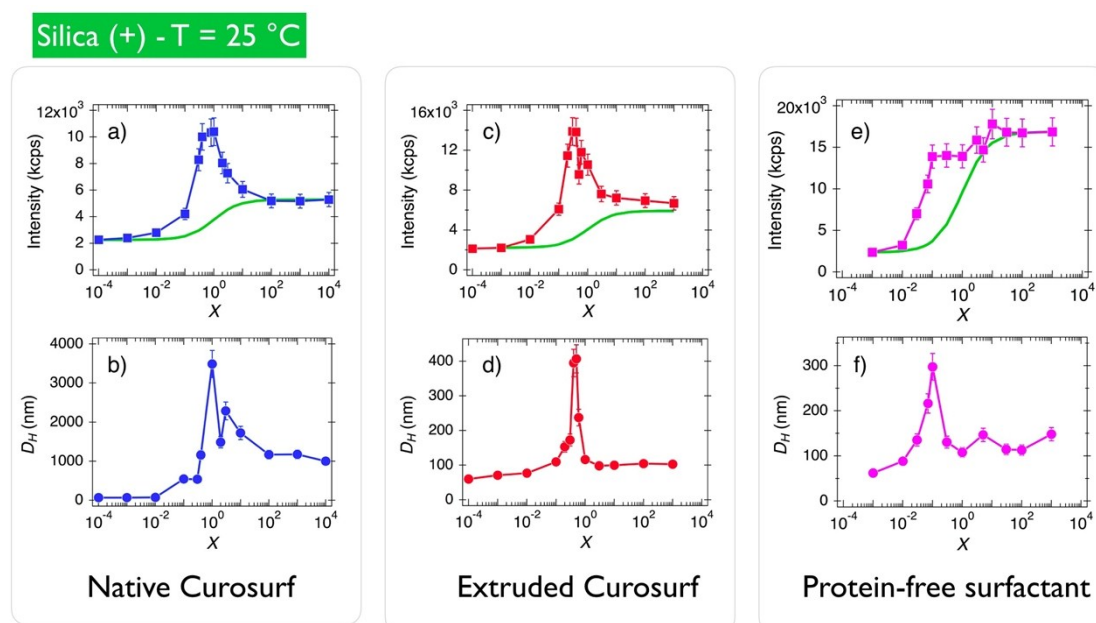
Figure S8.2: *Same as in Fig. S9.1 for Silica (+) particles.*

Figure S8.3: *Same as in Fig. S9.1 for Latex (+) particles.*

Figure S8.4: *Same as in Fig. S9.1 for Silica (-) particles.*

Latex (-) - T = 25 °C

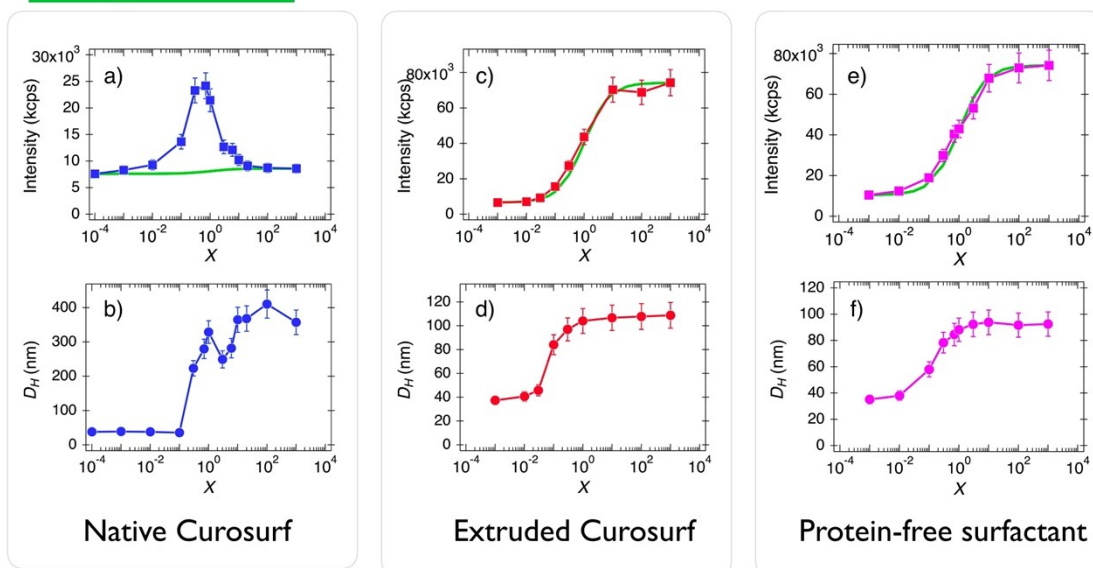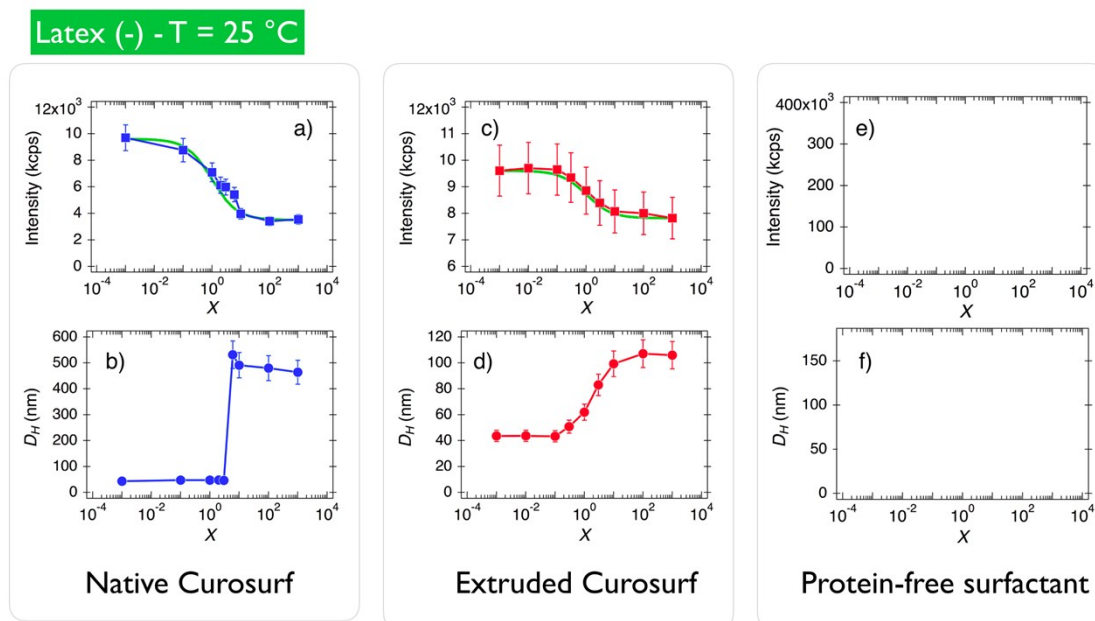**Figure S8.5:** *Same as in Fig. S9.1 for Latex (-) particles.*

Supplementary Information Figure S9 – Job scattering plots of nanoparticle/vesicle dispersions at 37 °C
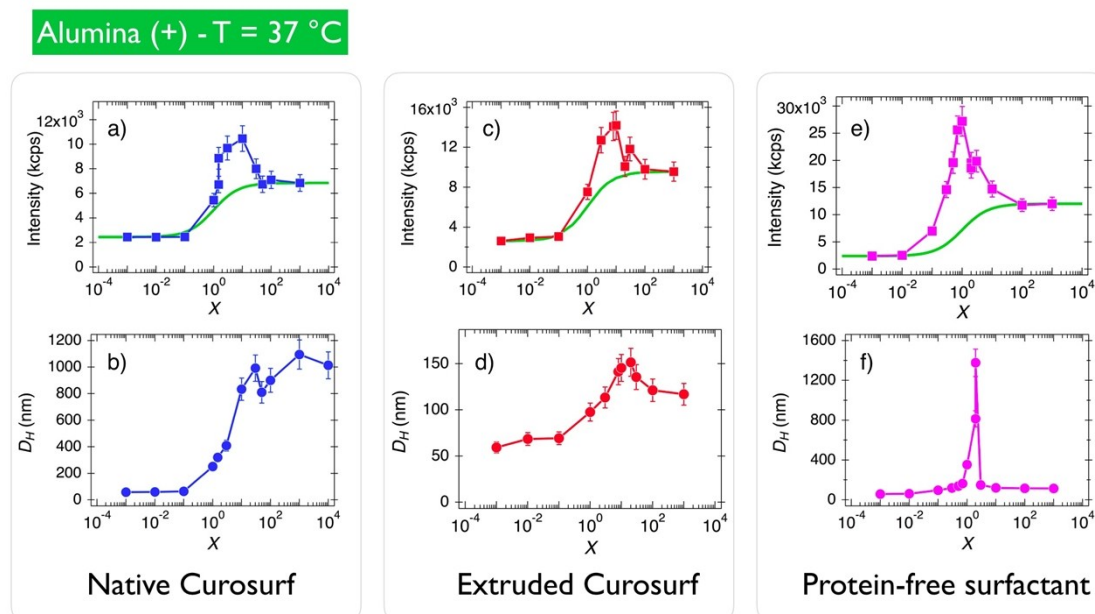

Figure S9.1: *Scattered intensity (a, c and e) and hydrodynamic diameter (b, d and f) of alumina particles mixed with native Curosurf® (a, b), extruded Curosurf® (c, d) and protein-free surfactant and (e, f) as a function of X (T = 37 °C). X is the ratio between the surfactant and nanoparticles weight concentration. The error bars represent the mean of the standard deviations for measurements made in triplicate. Continuous lines in green in a, c and e represent the scattered intensities calculated assuming that particles and vesicles do not interact.*
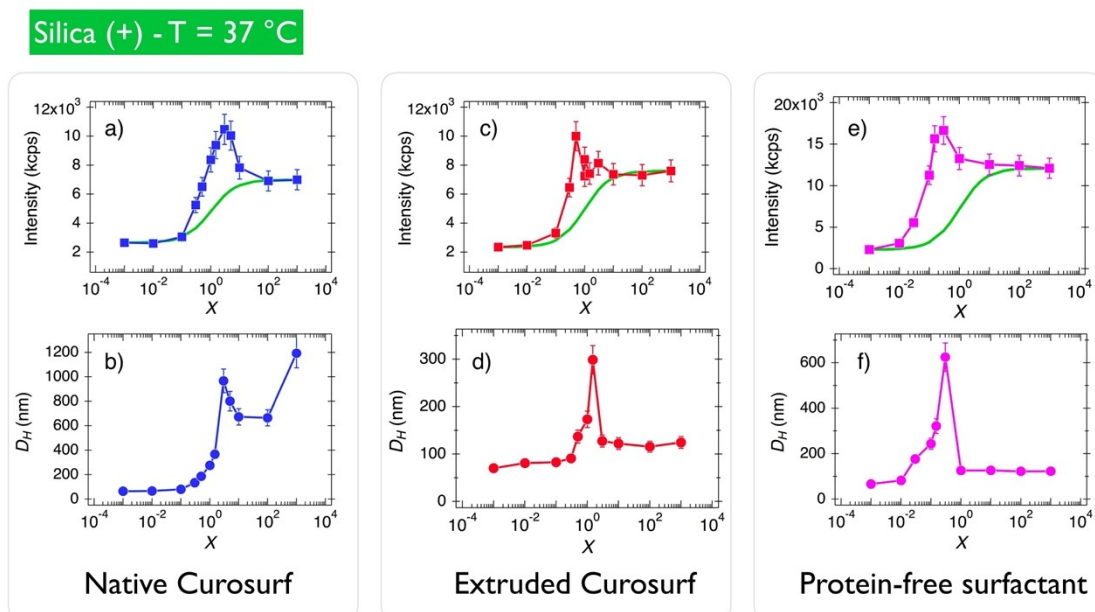

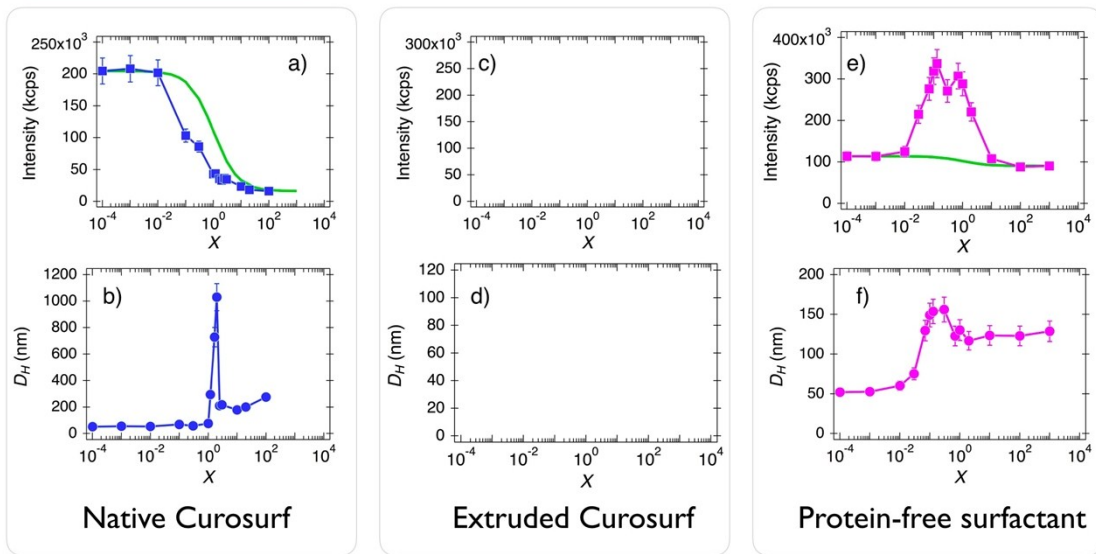**Figure S9.2:** *Same as in Fig. S10.1 for Silica (+) particles.*

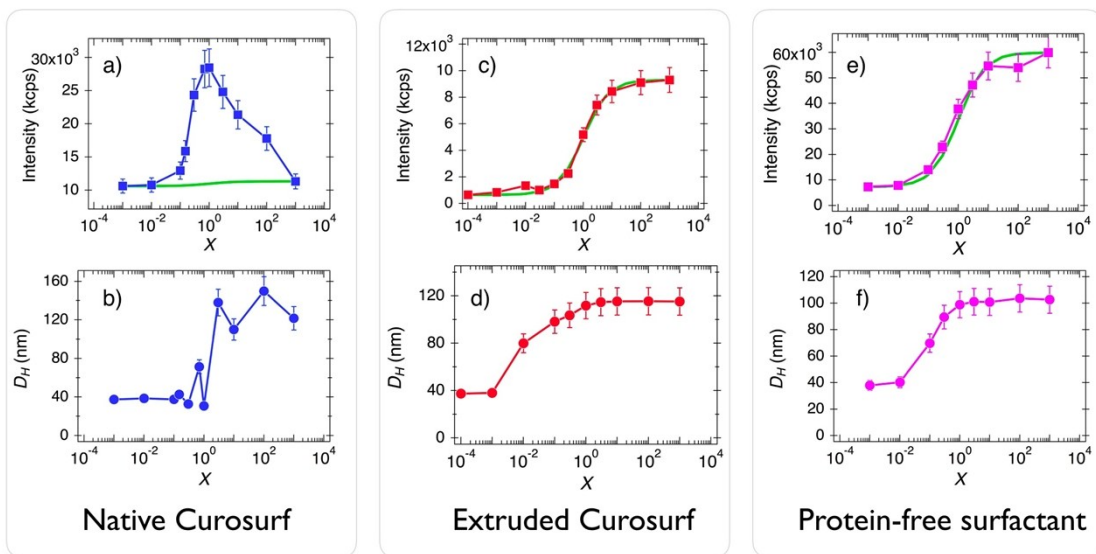**Figure S9.3:** *Same as in Fig. S10.1 for Latex (+) particles.*

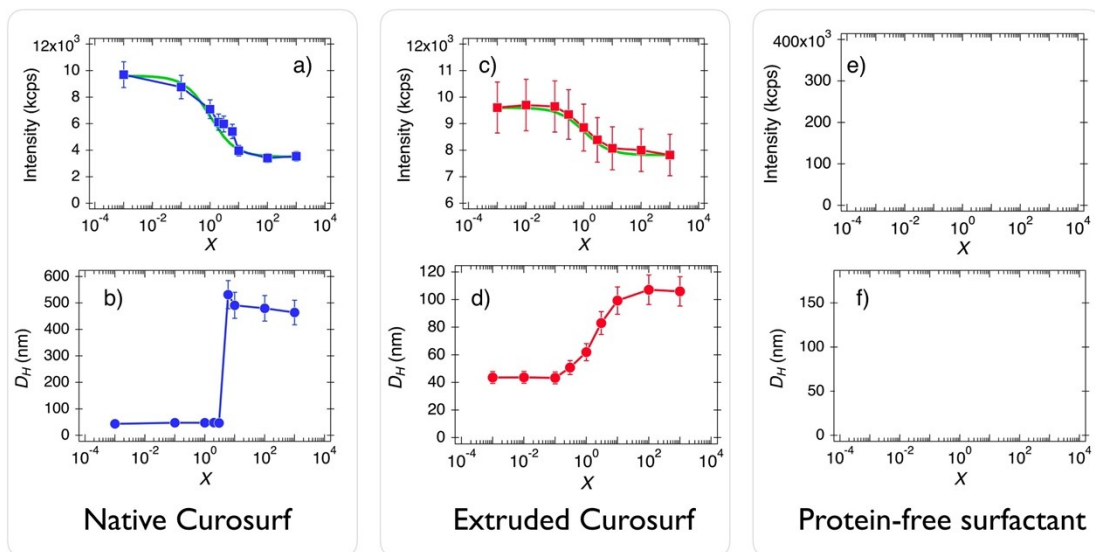**Figure S9.4:** *Same as in Fig. S10.1 for Silica (-) particles.*

Figure S9.5: *Same as in Fig. S10.1 for Latex (-) particles.*

Supplementary Information Figure S10 – Size distribution of nanoparticle-vesicle aggregates monitored by optical microscopy
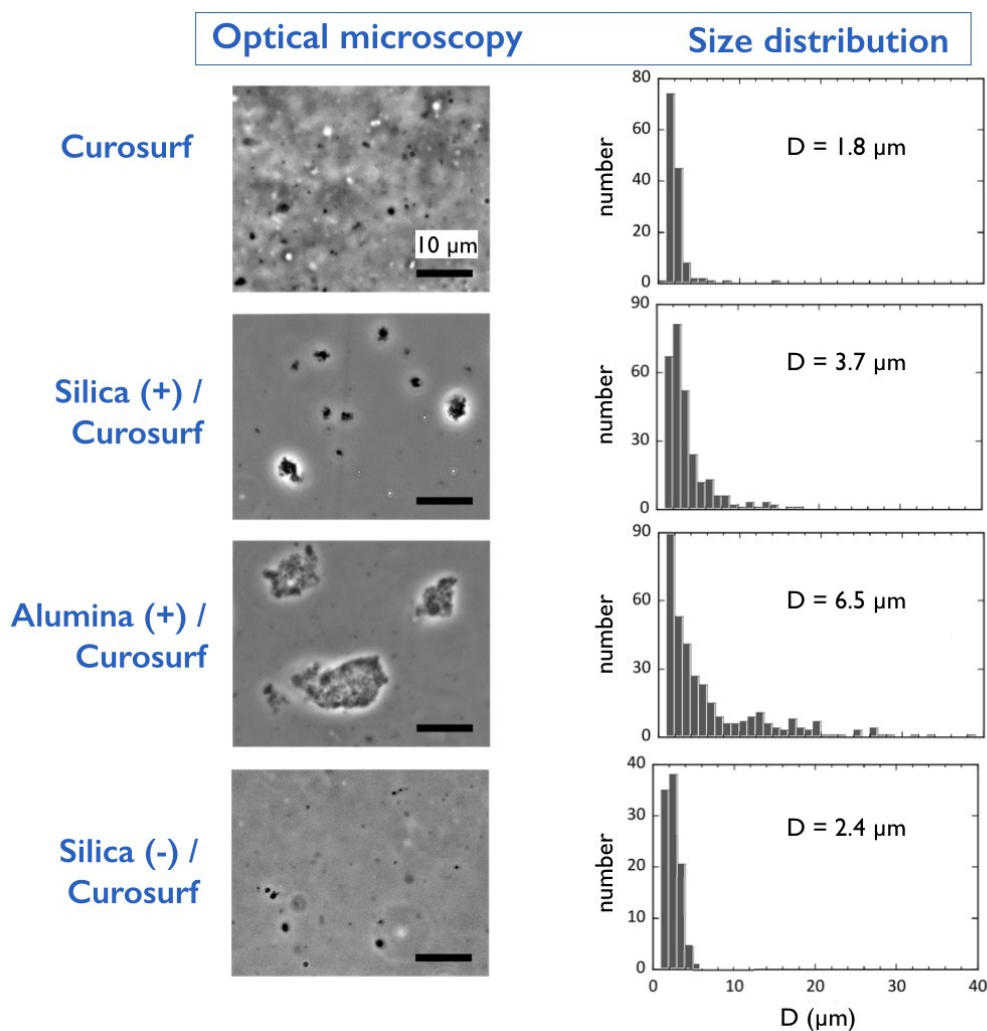

Figure S10: *Left-hand side*: phase-contrast optical microscopy images of mixed dispersions obtained from nanoparticles (Silica (+), Alumina (+) and Silica (-)) and Curosurf® at the mixing ratio X corresponding to the maximum seen in light scattering. The experimental conditions are T = 25 °C and c = 1 g L^{-1}. *Right-hand side*: size distribution derived from these and other microscopy images.

Supplementary Information S11 – Additional fluorescence optical microscopy images of Silica (+) – Curosurf® aggregates
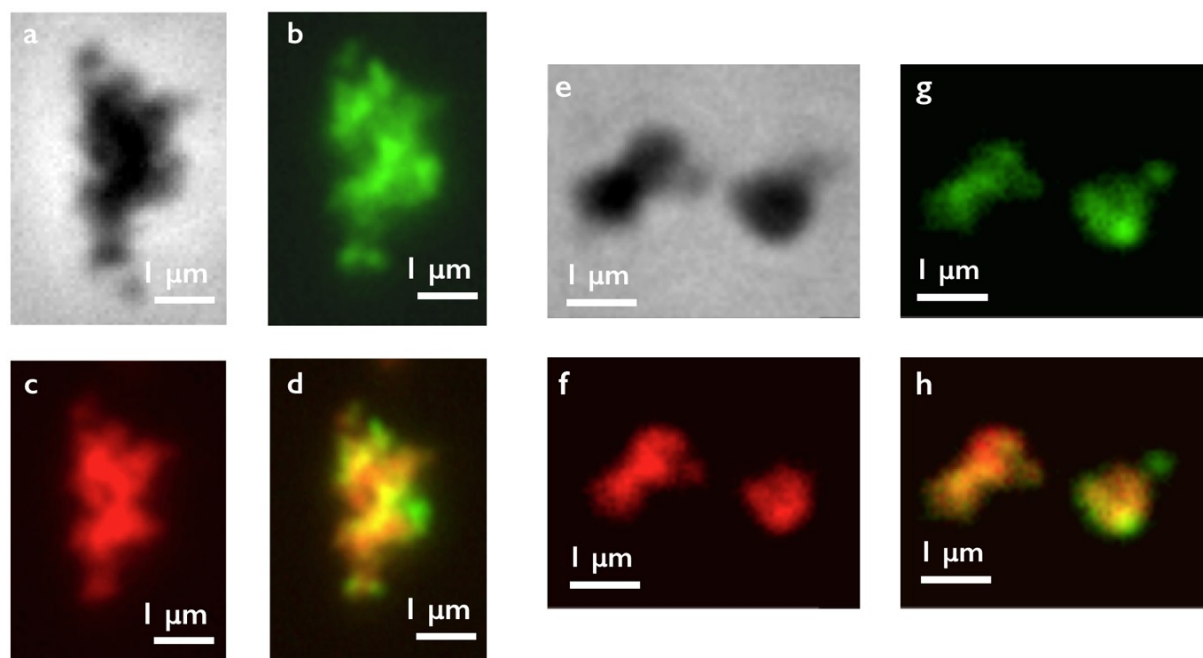

Figure S11: Close views of aggregates made from 40 nm aminated silica nanoparticles and native Curosurf® observed by optical and fluorescence microscopy (magnification 60×). The experimental conditions are c = 1 g L^{-1}, X = 2 and T = 37 °C. The Silica (+) are synthesized to fluoresce in the orange-red at 590 nm and the vesicles are labeled with a green fluorescent lipid (PKH67) emitting at 502 nm. The aggregates are observed under phase contrast (**a, e**), green (**b, g**) and red (**c, f**) illumination. The merge signals are shown in (**d, h**).

References

[1] A. Braun, P.C. Stenger, H.E. Warriner, J.A. Zasadzinski, K.W. Lu, H.W. Taeusch, A freeze-fracture transmission electron microscopy and small angle X-ray diffraction study of the effects of albumin, serum, and polymers on clinical lung surfactant microstructure, *Biophys. J.*, **93** (2007) 123-139.

[2] F. Mousseau, C. Puisney, S. Mornet, R. Le Borgne, A. Vacher, M. Airiau, A. Baeza-Squiban, J.F. Berret, Supported pulmonary surfactant bilayers on silica nanoparticles: formulation, stability and impact on lung epithelial cells, *Nanoscale*, **9** (2017) 14967-14978.

[3] C. Schleh, C. Muhlfeld, K. Pulskamp, A. Schmiedl, M. Nassimi, H.D. Lauenstein, A. Braun, N. Krug, V.J. Erpenbeck, J.M. Hohlfeld, The effect of titanium dioxide nanoparticles on pulmonary surfactant function and ultrastructure, *Respir. Res.*, **10** (2009) 90.

[4] F. Mousseau, R. Le Borgne, E. Seyrek, J.-F. Berret, Biophysicochemical Interaction of a Clinical Pulmonary Surfactant with Nanoalumina, *Langmuir*, **31** (2015) 7346-7354.

[5] F. Mousseau, L. Vitorazi, L. Herrmann, S. Mornet, J.F. Berret, Polyelectrolyte assisted charge titration spectrometry: Applications to latex and oxide nanoparticles, *J. Colloid Interface Sci.*, **475** (2016) 36-45.

[6] J.-F. Berret, Stoichiometry of electrostatic complexes determined by light scattering, *Macromolecules*, **40** (2007) 4260-4266.

[7] J. Fresnais, C. Lavelle, J.-F. Berret, Nanoparticle Aggregation Controlled by Desalting Kinetics, *J. Phys. Chem. C*, **113** (2009) 16371-16379.

[8] L. Qi, A. Sehgal, J.C. Castaing, J.P. Chapel, J. Fresnais, J.-F. Berret, F. Cousin, Redispersible hybrid nanopowders: Cerium oxide nanoparticle complexes with phosphonated-PEG oligomers, *ACS Nano*, **2** (2008) 879-888.